Effect of Arc Energy on Morphology and Microstructure of Laser-MIG Hybrid Welded Joints of Invar Alloy

*ZHAO Jiayi**, *GAO Qiyu*, *ZHANG Jiahao*, *ZHAN Xiaohong*

College of Materials Science and Technology, Nanjing University of Aeronautics and Astronautics, Nanjing 211106, P. R. China

(Received 22 April 2022; revised 6 July 2022; accepted 11 July 2022)

Abstract: Laser-MIG hybrid welding experiments of 7 mm thick Invar alloy are carried out. The macro appearance of joints is observed and the influence of arc energy on the cross-section morphology is analyzed. The distribution of temperature field is simulated to explain the relationship between heat effect and microstructure. Besides, the average grain size of weld under different arc energies is quantitatively studied. The results indicate that welded joints with uniformity and good formation are obtained. The weld width and the weld seam area increase and the depth to width ratio decreases with the increase of arc heat input. The transition of columnar crystals to equiaxed crystals is observed from the fusion line to the weld center. It is found that the higher the arc energy, the coarser the columnar crystal.

Key words: Invar alloy; laser-MIG hybrid welding; arc heat input; macro morphology

CLC number: TG456 **Document code:** A **Article ID:** 1005-1120(2022)S-0051-08

0 Introduction

Invar alloy, characterized by low thermal expansion coefficient and excellent mechanical properties, has been widely used as a potential mold material with high reliability and stability[1-2]. Based on these features, Invar alloy has extensive applications in aerospace industry, precision instrument manufacture, LNG tanker and other fields[3].

For the joining of thick Invar alloy plates, several common welding technologies, such as metal inert gas welding (MIG) or laser beam welding (LBW), have certain limitations[4-5]. The high welding heat input introduced by MIG process will lead to severe welding deformation, significant residual stress and grain coarsening.

Laser welding has been considered as a potential welding technique for its high energy density, fast welding speed, small distortion and so on. But welding defects like porosity or crack and poor gap adaptability are unavoidable problem.

The hybrid laser-arc welding technology, combining the advantages of advanced laser heat source and traditional arc heat source, has the advantages of lower heat input, deeper penetration, better bridging capacity and higher welding efficiency, and has better mechanical properties compared with the individual process[6-7]. At present, laser-arc welding has become one of the most promising methods for thick Invar alloy plate welding.

In recent years, more and more attention has been paid to numerical simulation techniques for studying the temperature field or the thermal history of the welding process[8-9].

This paper presents a comprehensive study of weld geometry, microstructure distribution and temperature field characteristics for laser-MIG welding Invar alloy under different arc energy through experimental and numerical methods. The weld dimension and grain size are measured. The microstructure in different regions which experience different thermal effect is briefly studied, and special attention is focused on the influence of arc energy on the molten pool morphology and the thermal cycle process.

*Corresponding author, E-mail address: zhaojiayi0602@163.com.

How to cite this article: ZHAO Jiayi, GAO Qiyu, ZHANG Jiahao, et al. Effect of arc energy on morphology and microstructure of laser-MIG hybrid welded joints of Invar alloy[J]. Transactions of Nanjing University of Aeronautics and Astronautics, 2022, 39(S): 51-58.

http://dx.doi.org/10.16356/j.1005-1120.2022.S.007

1 Experiment

1.1 Materials and equipment

The base metal (BM) adopted in this investigation is Invar alloy plates machined to the dimension of 100 mm×100 mm×7 mm without groove. The Invar M93 filler wire with a diameter of 1.2 mm is used during the laser-MIG experimental process. The chemical compositions of Invar alloy base metal and Invar M93 filler wire are shown in Table 1.

Table 1 Chemical compositions of Invar alloy base metal and Invar M93 filler wire (mass fraction) %

Material	Ni	C	Si	Mn	P	S	Cr	Co	Fe
Base metal	35.0—37.0	≤0.05	≤0.3	≤0.6	≤0.02	≤0.02	≤0.15	≤0.4	Bal.
Invar M93	36.2		0.53	0.55			0.23		Bal.

The experimental equipment includes KUKA Robot KR30HA, Fronius TPS-5000 welding machine and IPG YLS-6000 fiber laser, which are shown in Fig.1. And the schematic diagram of laser-MIG hybrid welding is presented in Fig.2.

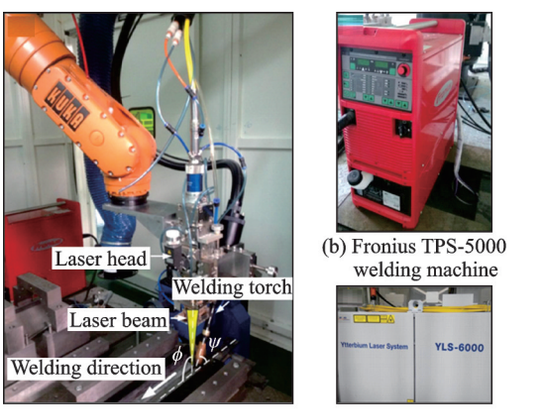

(a) KUKA Robot KR30HA (b) Fronius TPS-5000 welding machine (c) IPG YLS-6000 fiber laser

Fig.1 Laser-MIG experimental equipment

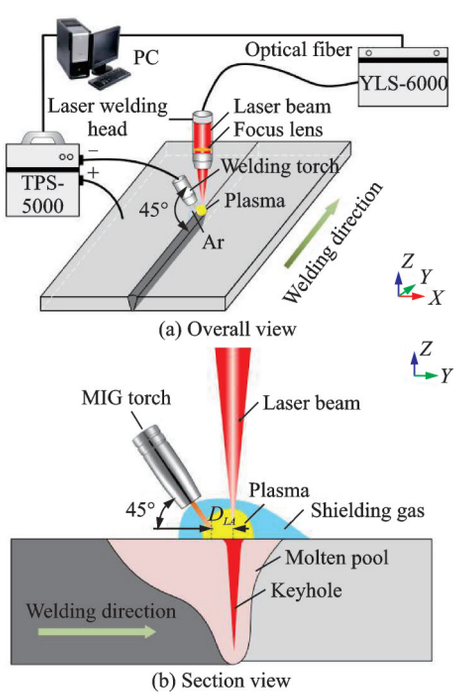

(a) Overall view

(b) Section view

Fig.2 Schematic diagram of laser-MIG experiment

1.2 Design of experiment

In the laser-MIG welding process, the laser beam is perpendicular to the workpiece and the angle of welding torch to the workpiece surface is 45°. A laser-arc distance of 3 mm is selected to ensure the coupling effect between laser heat source and arc heat source. The 99.99% argon gas with a flow rate of 15 L/min is used as the shielding gas, which shows a good protective performance in the experiment. Besides, the defocus amount applied is 0 mm. Detailed experiment parameters are shown in Table 2.

Table 2 Welding parameters in the experiment

No.	Laser power/ W	Welding speed/ (m•min^{-1})	Welding current/ A	Welding voltage/ V	Arc energy/ (kJ•m^{-1})
1	3 000	1	152	18.7	170.5
2	3 000	1	200	22.2	266.4
3	4 000	1	200	22.2	266.4
4	4 000	1	152	18.7	170.5

1.3 Sample preparation

Before the welding process, the oxide film of the specimen surface is removed by the milling machine, and then the specimen surface is washed with acetone to eliminate contaminants. After the welding experiment, the metallography samples are cut from weldments by wire-electrode cutting. The metallurgical specimens are grinded and polished by abrasive paper and metallographic polisher. After that, the metallurgical surfaces are etched with a corrosive reagent which contains 8% HF, 15% HNO_3, 2% H_3BO_3 and 75% H_2O to reveal the microstructure. The microstructure of the weld is ob-

served by MR-5000 optical microscope.

2 Modeling

In order to explain the relationship between the thermal history and the microstructure of laser-MIG welded joints, a numerical model is developed to investigate the temperature distribution of the weld. In this study, the model is solved by the finite element method and the simulation is conducted by the software MSC.Marc. Fig.3 shows the geometry model and meshing results.

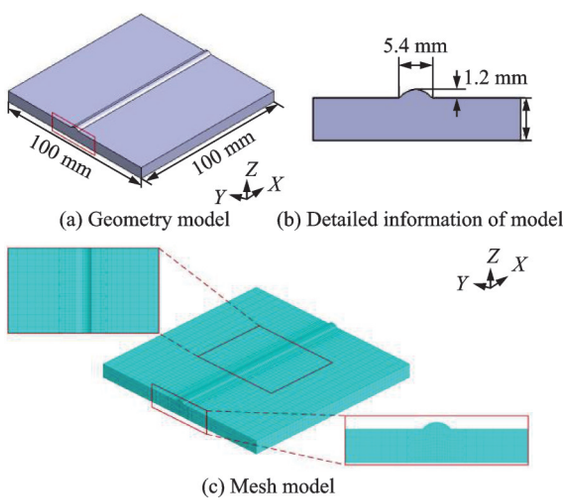

Fig.3 Geometry model and meshing of the model

For ensuring the accuracy of simulation and improving the computing efficiency, a grid meshing method which allows finer mesh in the welded zone and coarser mesh in the non-welded zone is performed. The component is ultimately meshed into 27 048 mesh elements with 34 388 nodes. In this paper, the minimum size of meshes is 1 mm×0.6 mm×0.5 mm, and the maximum is 5 mm×2 mm×1.5 mm.

A double-ellipsoid heat source (manifested in Fig.4(a)) is used to simulate the effect of arc and its expression is described by

$$q_1(x,y,z)=\frac{6\sqrt{3}\,f_1Q_r}{\pi^{\frac{3}{2}}a_1bc}\exp\left(-3\left[\left(\frac{x}{a_1}\right)^2+\left(\frac{y}{b}\right)^2+\left(\frac{z}{c}\right)^2\right]\right) \quad (1)$$

$$q_2(x,y,z)=\frac{6\sqrt{3}\,f_2Q_r}{\pi^{\frac{3}{2}}a_2bc}\exp\left(-3\left[\left(\frac{x}{a_2}\right)^2+\left(\frac{y}{b}\right)^2+\left(\frac{z}{c}\right)^2\right]\right) \quad (2)$$

where $q_1(x,y,z)$ are $q_2(x,y,z)$ are the heat flux density of the rear and front part ellipsoid, respectively; Q_r is the heat input of arc; a_1, a_2, b and c are the parameters to describe the shape of double ellipsoid, and f_1 and f_2 are the energy distribution coefficients and meet $f_1+f_2=2$.

A combined heat source consisting of Gauss surface heat source and Gauss cylinder body heat source (manifested in Fig.4(b)) is used to simulate the effect of laser. The expressions of the heat flux density for the Gauss surface heat source $q_s(x,y)$ and the Gauss cylinder body heat source $q_v(x,y)$ can be described as follows

$$q_s(x,y)=\frac{\alpha Q_s}{\pi r_s^2}\exp\left[-\frac{\alpha(x^2+y^2)}{r_s^2}\right] \quad (3)$$

$$q_v(x,y)=\frac{6Q_v(H-\beta h)}{\pi r_v^2H^2(2-\beta)}\exp\left[\frac{-3(x^2+y^2)}{r_v^2}\right] \quad (4)$$

where α is the concentration coefficient of the surface heat flux, H the depth of the body heat source, and β the attenuation coefficient; Q_s and Q_v are the power of the surface and body heat source, respectively, and r_s and r_v the effective radius of the surface and body heat source, respectively.

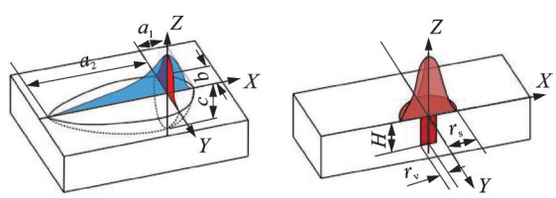

Fig.4 Models of arc heat source and laser heat source

The relationship of Q_s and Q_v is subjected to the following formula

$$Q_l\eta=Q_s+Q_v \quad (5)$$

where Q_l is the heat input of laser and η the effective heat absorption coefficient.

The thermal properties of the material have a great influence on the accuracy of simulation, and the parameters required are presented in Fig.5.

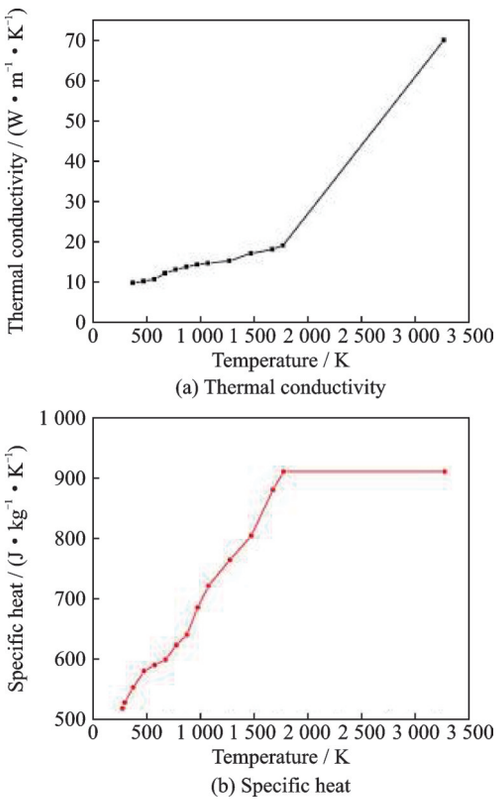

Fig.5 Thermal properties of Invar alloy

3 Results and Discussion

3.1 Macro morphology

Fig.6 shows surface profile and cross section of welds produced by laser-MIG hybrid welding with different arc energy. The appearance of welds has great uniformity and only few splashes can be observed around weld seam. The cross section of joints exhibits an asymmetric goblet shape. There are several porosities scattered on the cross section, and mainly concentrated at the bottom of weld seam. Most of porosities present regular circular morphology generally induced by the collapse of keyhole.

The corresponding statistics of weld width, depth, depth to width and area of joints are shown in Fig.7. With constant laser energy of 4 000 W, greater weld width (6.78 mm) and weld seam area (18.13 mm^2) are obtained with higher arc energy, while the value of fusion depth and weld depth to width show a declining trend with the increase of arc energy. The above results suggests that arc energy exerts a significant influence on the increase of weld width but little influence on the penetration ability of laser-MIG hybrid welding.

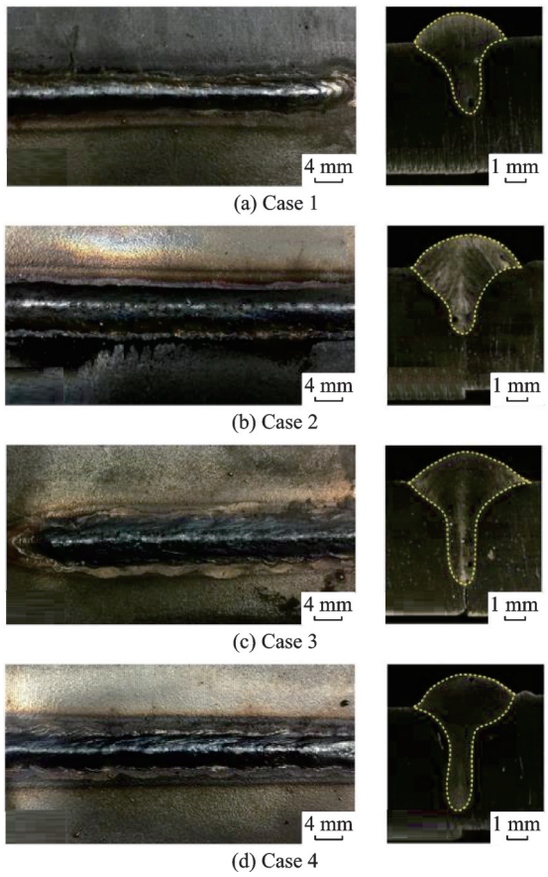

Fig.6 Surface profile and cross-section morphology of laser-MIG welded joints

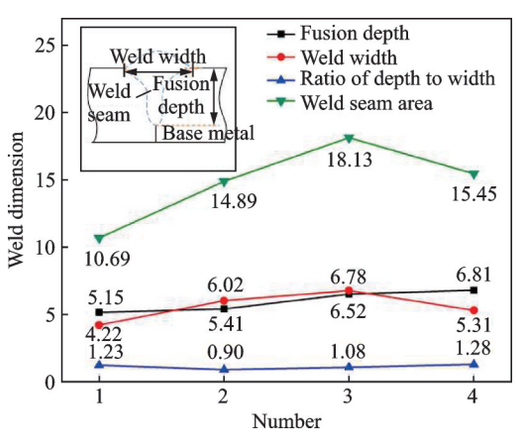

Fig.7 Variation of weld geometries (unit: mm)

3.2 Microstructure

Fig.8 shows macro profile and microstructure of different areas in the weld seam. The microstructure in the region near the top surface is composed of coarse equiaxed grains. Coarse columnar crystals are found in the region adjacent to the fusion line and the growth orientations of crystals are perpendic-

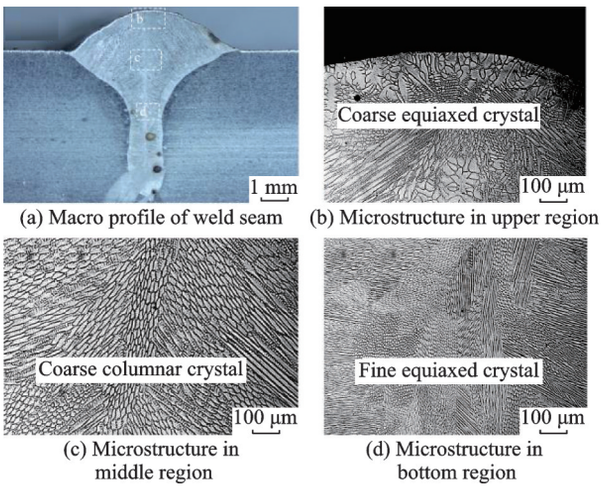

(a) Macro profile of weld seam (b) Microstructure in upper region (c) Microstructure in middle region (d) Microstructure in bottom region

Fig.8 Macro profile and microstructure of different areas in the weld seam

ular to it. From the fusion line to the center of weld seam, columnar crystals are gradually transformed into equiaxial crystals. Due to the effect of different thermal cycles, the grain size along the center line varies greatly. The grain size in the upper region of the weld seam which is regarded as laser-arc dominated region is much coarser than that in the bottom region which is regarded as laser dominated region.

For studying the effect of arc energy on grain morphology, grain size of the columnar crystal is calculated by counting the number of columnar crystals in per unit length. As shown in Figs.9 and 10, two individual areas are selected for the measurement. Grain size for Case 3 of the average columnar crystal fabricated under higher arc energy is 8.71 μm, while that for Case 4 fabricated under

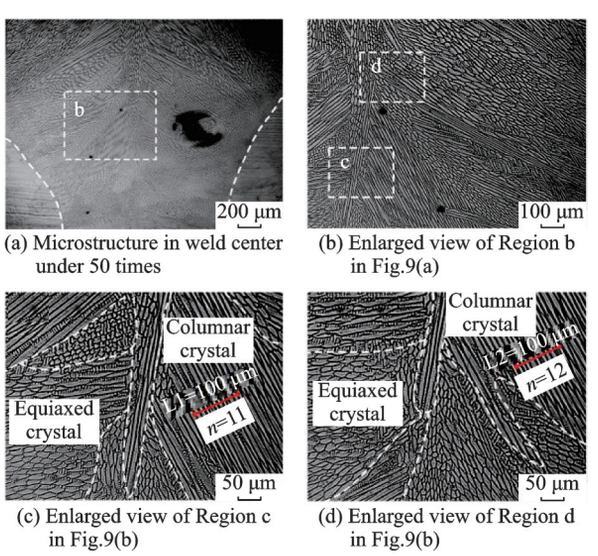

(a) Microstructure in weld center under 50 times (b) Enlarged view of Region b in Fig.9(a) (c) Enlarged view of Region c in Fig.9(b) (d) Enlarged view of Region d in Fig.9(b)

Fig.9 Grain size in weld seam region for Case 3

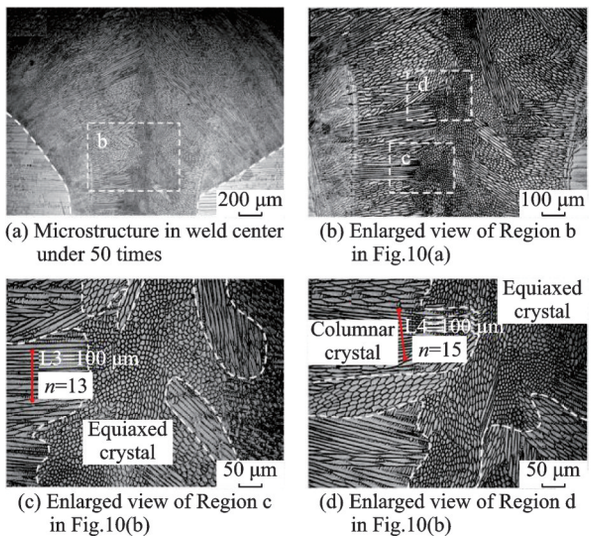

(a) Microstructure in weld center under 50 times (b) Enlarged view of Region b in Fig.10(a) (c) Enlarged view of Region c in Fig.10(b) (d) Enlarged view of Region d in Fig.10(b)

Fig.10 Grain size in weld seam region for Case 4

smaller arc energy is 7.18 μm. It is explained that increasing arc energy results in longer lasting time in high temperature and slower cooing rate, which provides sufficient conditions for grain nucleation and growth.

3.3 Temperature field numerical analysis

To investigate the relation between thermal effect and evolved microstructure and the influence of arc energy on molten pool morphology, the temperature field is simulated. First, the correctness of the heat source model is verified by comparing the simulated and experimental results. It is shown in Fig.11 that the simulated molten pool appearance has a good agreement with the practical weld cross section.

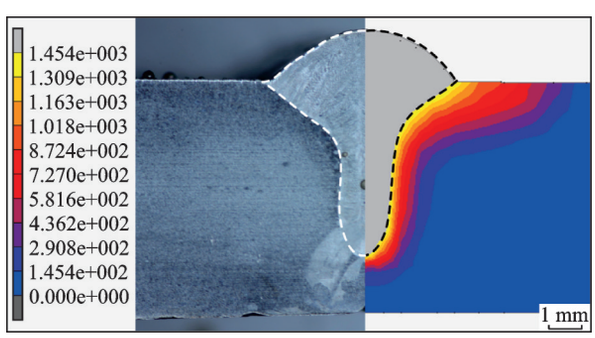

Fig.11 Calibration results of heat source

Fig.12 shows the molten pool appearance in different sections during laser-MIG welding process. In the laser-MIG process, a keyhole is formed induced by the effect of laser. At the same time, filling wire is melted under the effect of arc, forming

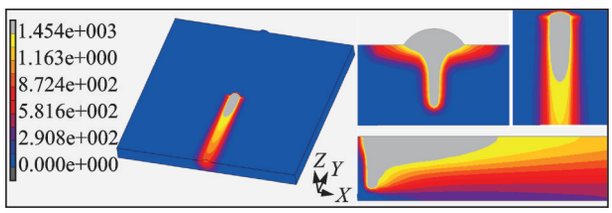

Fig.12 Molten pool shape at $T = 3$ s

droplets and entering the molten pool, and finally causing the weld reinforcement. In the top view, the molten pool is a semi-ellipsoid with large length to width ratio. In front of the molten pool, which is mostly affected by laser, the isotherm is dense and the temperature gradient is large. While the rear side of the molten pool is mostly affected by arc, the isotherm is relatively sparse and temperature gradient is smaller.

The grain morphology is greatly determined by temperature gradient and crystallization rate. Fig.13 shows the temperature and temperature gradient distribution along the center line of weld seam. From the weld surface to the bottom, the temperature shows an obvious downward trend and the temperature gradient experiences a process of rising first, falling subsequently and close to 0 at final.

In the initial stage of solidification, the bottom molten pool solidifies first. Because the temperature gradient in this region is close to 0, it nucleates and mostly grows into equiaxed crystals. The temperature at the bottom is hardly affected by arc, so the lowest temperature is obtained. The grain growth is limited under the low heat input, so fine equiaxed crystals are formed. The columnar grains formed in the middle region result from the large solidification rate and grain size increases due to the coupled heat effect of laser and arc. The temperature gradient

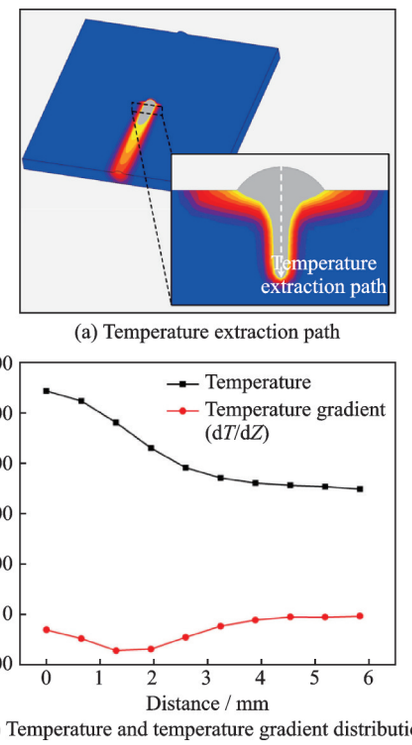

Fig.13 Temperature and temperature gradient distributions in specific path

near the surface decreases and equiaxed crystals are formed. However, the temperature reaches the maximum, so the grain will further coarsen.

Fig.14 manifests the temperature field under different arc energy. As shown in Fig.14(a), when influenced only by individual laser heat source, the molten pool formed is ellipse shape and relatively small due to the highly concentrated laser energy. When arc heat is introduced, the range of temperature field of the hybrid welding is significantly larger than that of the laser welding because the action range of arc is larger than the laser. As arc energy increases, the molten pool shape becomes wider and the isotherm becomes sparser.

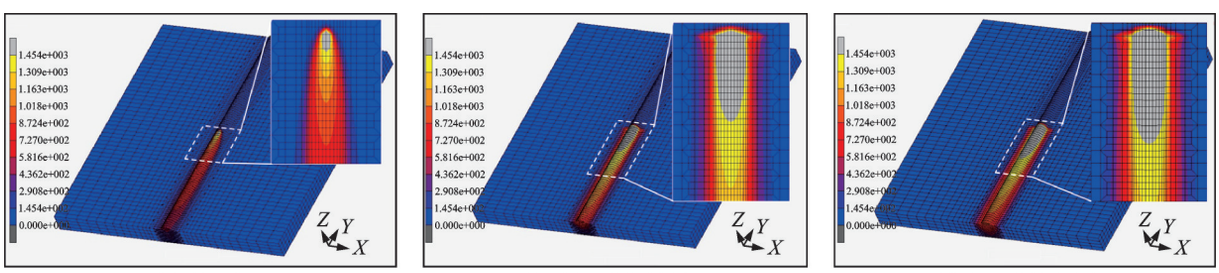

Fig.14 Temperature field under different arc energy

In order to study the effect of arc energy on the thermal cycle process, the thermal cycle curve of two nodes along the weld centerline is extracted respectively. As shown in Fig.15(b), the peak temperature of Node 1 increases from 2 578 ℃ to 2 790 ℃ and 3 062 ℃ with the continuous increase of arc energy from 0 to 170.5 kJ/m and 266.4 kJ/m. However, it can be concluded from Fig.15(c) that the peak temperature of Node 2 has been stable around 2 482 ℃ regardless of arc energy, indicating that arc heat has little thermal effect on the bottom weld seam.

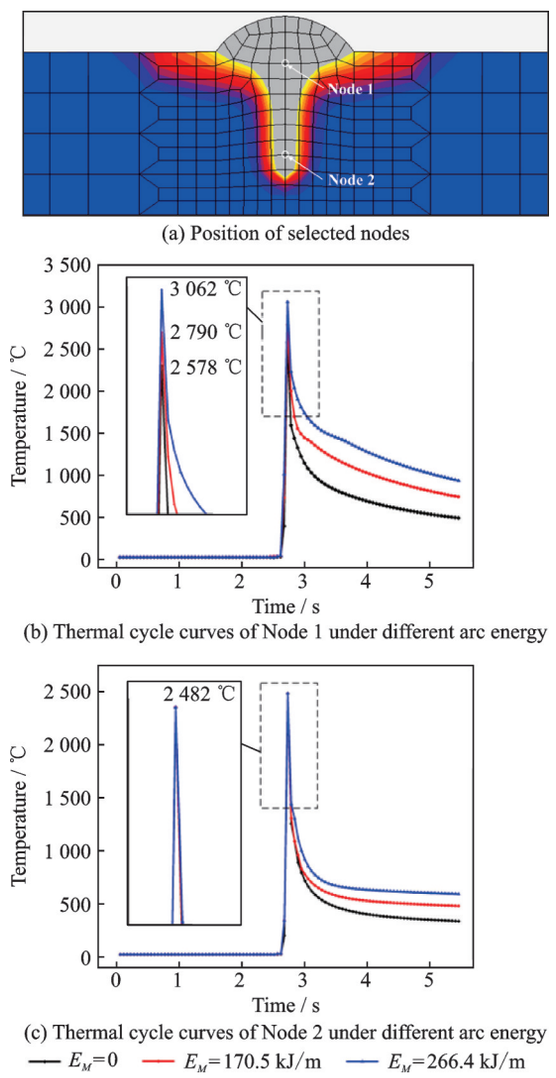

Fig.15 Thermal cycle curves of different positions

4 Conclusions

Laser-MIG hybrid welding of Invar alloy with different arc energy is performed. The influence of arc energy on weld appearance, molten pool shape and thermal cycle process is investigated. The grain size under different arc heat inputs is measured. Besides, the interrelation between thermal effect and microstructure is explained by studying the temperature field. The conclusions can be achieved as follows:

(1) The appearance of the weld surface is clean and uniform. The cross section of weld is basically "goblet" shape with wider width at the surface and narrower width at the bottom. The porosities are mostly located in the laser dominated region. With the increase of arc energy, the weld width and weld seam area show an ascending trend and the depth to width ratio shows a descending trend.

(2) The microstructure of the weld seam consists of much columnar crystals and less equiaxed crystals. From the fusion line to weld center, there is a trend of columnar crystals transformed to equiaxed crystals. From the surface to the bottom of the weld, the microstructure changes from coarse equiaxed crystals to coarse columnar crystals in the middle and fine equiaxed crystals in the bottom. It is found that grain size of the columnar crystal decrease with the decline of arc energy.

(3) The grain dimension and morphology in different areas is related to the corresponding temperature and temperature gradient. The simulated temperature field indicates that the increasing arc energy results in wider molten pool and sparser isotherm. Arc energy has a great effect on the thermal cycle process in the upper region of the weld but little on that in the bottom weld.

References

[1] SAHOO A, MEDICHERLA V R R. Fe-Ni Invar alloys: A review[J]. Materials Today: Proceedings, 2021, 43(2): 2242-2244.

[2] SHIGA M. Invar alloys[J]. Current Opinion in Solid State and Materials Science, 1996, 1(3): 340-348.

[3] YANG Q D, WEI K, YANG X J, et al. Microstructures and unique low thermal expansion of Invar36 alloy fabricated by selective laser melting[J]. Materials Characterization, 2020, 166: 110409.

[4] ZHAN X H, LI Y B, OU W M, et al. Comparison

between hybrid laser-MIG welding and MIG welding for the Invar36 alloy[J]. Optics & Laser Technology, 2016, 85: 75-84.

[5] LIU F Y, TAN C W, GONG X T, et al. A comparative study on microstructure and mechanical properties of HG785D steel joint produced by hybrid laser-MAG welding and laser welding[J]. Optics & Laser Technology, 2020, 128: 106247.

[6] ZHAN X H, ZHANG D, WEI Y H, et al. Research on the microstructure and properties of laser-MIG hybrid welded joint of Invar alloy[J]. Optics & Laser Technology, 2017, 97: 124-136.

[7] ACHERJEE B. Hybrid laser arc welding: State-of-art review[J]. Optics & Laser Technology, 2018, 99: 60-71.

[8] CHEN S, WU Y F, LI Y. Study on 2219 Al-Cu alloy T-joint used dual laser beam bilateral synchronous welding: Parameters optimization based on the simulation of temperature field and residual stress[J]. Optics & Laser Technology, 2020, 132: 106481.

[9] SUN G F, WANG Z D, LU Y, et al. Numerical and experimental investigation of thermal field and residual stress in laser-MIG hybrid welded NV E690 steel plates[J]. Journal of Manufacturing Processes, 2018, 34: 106-120.

Author Ms. **ZHAO Jiayi** received the B.S. degree in metallic materials engineering from Nanjing Tech University in 2020. She became a postgraduate student in Nanjing University of Aeronautics and Astronautics in September 2020. Her research is focused on the laser-MIG welding technology of Invar alloy.

Author contributions Ms. **ZHAO Jiayi** designed the experiment, conducted the analysis, and wrote the manuscript. Dr. **GAO Qiyu** contributed to the data anlysis and discussion of the study. Dr. **ZHANG Jiahao** contributed to the experimental preparation and model development. Prof. **ZHAN Xiaohong** revised and polished the manuscript. All authors commented on the manuscript draft and approved the submission.

Competing interests The authors declare no competing interests.

(Production Editor: XU Chengting)

电弧能量对Invar合金激光-MIG复合焊接头形貌与显微组织的影响研究

赵佳怡，高奇玉，张家豪，占小红

(南京航空航天大学材料科学与技术学院，南京 211106，中国)

摘要：开展了7 mm厚Invar合金激光-MIG复合焊接实验，对接头的宏观形貌进行了观察，并分析了电弧能量对横截面形貌的影响。通过模拟温度场分布解释了焊接热效应与微观组织的关联关系。除此之外，定量研究了不同电弧热输入下焊缝的晶粒度大小。结果表明，形成焊缝具有良好的均匀性与成形，随着电弧热输入量的增加，焊缝熔宽及焊缝面积增加，深宽比有所减小。从熔合线到焊缝中心可以观察到柱状晶逐渐转变为等轴晶。同时发现电弧能量越大，柱状晶越粗。

关键词：Invar合金；激光-MIG复合焊；电弧热输入；宏观形貌